

# Experimental study on the capillary thinning of entangled polymer solutions

Dirk Sachsenheimer · Bernhard Hochstein ·  
Norbert Willenbacher

Received: 14 February 2014 / Revised: 27 June 2014 / Accepted: 10 July 2014 / Published online: 1 August 2014  
© Springer-Verlag Berlin Heidelberg 2014

**Abstract** The transient elongation behavior of entangled polymer and wormlike micelles (WLM) solutions has been investigated using capillary breakup extensional rheometry (CaBER). The transient force ratio  $X = 0.713$  reveals the existence of an intermediate Newtonian thinning region for polystyrene and WLM solutions prior to the viscoelastic thinning. The exponential decay of  $X(t)$  in the first period of thinning defines an elongational relaxation time  $\lambda_x$  which is equal to elongational relaxation time  $\lambda_e$  obtained from exponential diameter decay  $D(t)$  indicating that the initial stress decay is controlled by the same molecular relaxation process as the strain hardening observed in the terminal regime of filament thinning. Deviations in true and apparent elongational viscosity are discussed in terms of  $X(t)$ . A minimum Trouton ratio is observed which decreases exponentially with increasing polymer concentration leveling off at  $Tr_{\min} = 3$  for the solutions exhibiting intermediate Newtonian thinning and  $Tr_{\min} \approx 10$  otherwise. The relaxation time ratio  $\lambda_e/\lambda_s$ , where  $\lambda_s$  is the terminal shear relaxation time, decreases exponentially with increasing polymer concentration and the data for all investigated solutions collapse onto a master curve irrespective of polymer molecular weight or solvent viscosity when plotted versus the reduced concentration  $c[\eta]$ , with  $[\eta]$  being the intrinsic viscosity. This confirms the strong effect of the nonlinear deformation in CaBER experiments on entangled polymer solutions as suggested earlier. On the other hand,  $\lambda_e \approx \lambda_s$  is found for all WLM solutions clearly indicating that these nonlinear

deformations do not affect the capillary thinning process of these living polymer systems.

**Keywords** CaBER · Filament stretching · Polymer solution · Wormlike micelles · Elongational viscosity · Relaxation time

## Introduction

Capillary breakup extensional rheometry (CaBER) is a common technique for the determination of the elongational behavior of low-viscosity fluids. This simple and versatile method has been suggested more than 20 years ago (Bazilevsky et al. 1990; Entov and Hinch 1997; Bazilevsky et al. 2001); and is commercially available (Haake CaBER 1, Thermo Scientific). In contrast to other techniques, CaBER allows for large Hencky strains up to  $\varepsilon_{\max} \approx 8\text{--}13$  which are of great significance to industrial practice. The CaBER experiment is based on the creation of an instable liquid bridge. After applying a step strain within a short strike time in a range of typically  $t_s \approx 20\text{--}100$  ms, the diameter of the liquid filament decreases due to the acting surface tension. Monitoring of the filament diameter as a function of time allows for the determination of characteristic elongational flow properties such as the apparent elongational viscosity (Anna and McKinley 2001a), the elongational relaxation time (Entov and Hinch 1997; Clasen 2010), or the elongational yield stress (Niedzwiedz et al. 2009; Niedzwiedz et al. 2010; Martinie et al. 2013).

In a commercial CaBER setup, the only measured quantity during filament thinning is the diameter decay  $D(t)$  at a single position in the filament. Different extensions of the experimental setup are reported in the literature such as optical shape recognition using a (high-speed) camera

D. Sachsenheimer (✉) · B. Hochstein · N. Willenbacher  
Institute for Mechanical Process Engineering and Mechanics,  
Group Applied Mechanics (AME), Karlsruhe Institute  
of Technology (KIT), Gotthard-Franz-Straße 3, 76131  
Karlsruhe, Germany  
e-mail: sachsenheimer@kit.edu

(Christanti and Walker 2001; Niedzwiedz et al. 2009; Nelson et al. 2011; Gier and Wagner 2012; Sattler et al. 2012), force measurement during initial step strain (Klein et al. 2009) as well as during the whole capillary thinning process (Sachsenheimer et al. 2012). Unfortunately, controlling the temperature of the thinning liquid thread is not possible due to the lack of an appropriate temperature control unit for CaBER and, therefore, capillary thinning is only performed at room temperature. In a study on polyacrylonitrile solutions, samples have been preheated and an elevated constant temperature was assumed due to the short time of experimentation although these measurements were done at room temperature (Tan et al. 2012). In contrast, extensional rheometry of polymer melts has been performed at elevated temperatures. The “universal extensional rheometer” of (Münstedt 1975, Münstedt 1979; Münstedt et al. 1998) stretches polymer melt filaments in a tempered silicon oil bath in order to maintain an accurate temperature control spatially as well as temporally. Furthermore, a filament stretching extensional rheometer (FiSER) has been equipped with an oven (Bach et al. 2003) in order to determine the elongational properties of polymer melts up to a temperature of  $T = 200^\circ\text{C}$ . The length of the filament is continuously increased; therefore, FiSER experiments require very large devices and an accurate temperature control is complicated due to convection in the oven. To reduce a vertical temperature gradient, (Bach et al. 2003) used six temperature transducers combined with eight heat elements as well as a nitrogen flow through the oven smearing out temperature gradients. To the best of our knowledge, no capillary thinning experiments under controlled temperature conditions other than room temperature have been reported so far.

The thinning behavior of a liquid thread is controlled by the capillary force and viscous or viscoelastic forces. The interplay of these forces results in characteristic diameter vs. time curves observed experimentally and predicted theoretically for different types of fluids, e.g., Bingham plastic, power law, Newtonian fluid, or viscoelastic fluid. However, the classical way of calculating the elongational viscosity from CaBER experiments is based on the assumption of vanishing axial normal stress (axial force is only caused by the surface tension). Recently, we introduced the so-called tilted CaBER method (Sachsenheimer et al. 2012) to determine the true axial force during the capillary thinning process. In this type of experiment, the filament is stretched horizontally and the axial force can be determined from gravity-driven bending of the filament in a range of  $F = 1,000\text{--}0.1 \mu\text{N}$ .

Using the CaBER technique, we want to improve our knowledge of the self-controlled thinning behavior of concentrated and mostly entangled polymer solutions. Therefore, we give first a brief introduction into the

theory of filament thinning and CaBER experiments of non-Newtonian fluids focusing on the elongational relaxation time and the true elongational viscosity. Then, we present the experimental setup and give a short overview of the samples used including preparation and characterization. Following with the experimental part, we analyze the effect of different geometrical setups. The transient force ratio including its effect on the elongational viscosity is discussed. After this, we discuss the elongational relaxation time and the relaxation time ratio including a universal scaling for polymer solutions. Finally, we compare CaBER results for some surfactant solutions with filament stretching (FiSER) experiments and give a short conclusion.

## Filament thinning and CaBER experiment

### Diameter vs. time evolution during capillary thinning

Newtonian fluids form nearly cylindrical filaments. The midpoint diameter  $D_{\text{mid}}$  of such a thread decreases linearly with time  $t$  in a CaBER experiment according to the following (Papageorgiou 1995; McKinley and Tripathi 2000):

$$D_{\text{mid}}(t) = D_1 - \Theta \frac{\Gamma}{\eta_s} t \quad (1)$$

where  $D_1$  is the initial diameter of the linear filament thinning region (this corresponds to time  $t = 0$  in the model equation),  $\Gamma$  is the surface tension,  $\eta_s$  is the shear rate-independent shear viscosity of the Newtonian liquid, and  $\Theta$  is a constant numerical factor. Neglecting inertia, Papageorgiou (1995) predicted  $\Theta = 0.1418$  which was confirmed experimentally (McKinley and Tripathi 2000; Sachsenheimer et al. 2012) for the capillary thinning of a Newtonian fluid.

Weakly viscoelastic fluids like dilute and semi-dilute solutions of linear, flexible polymers form perfect cylindrical filaments, and their diameter decreases exponentially with time in CaBER experiments (Bazilevsky et al. 1990; Renardy 1994, 1995; Brenner et al. 1996; Bazilevsky et al. 1997; Eggers 1997; Liang and Mackley 1994; Entov and Hinch 1997; Kolte et al. 1999; Anna and McKinley 2001a; Rodd et al. 2005; McKinley 2005; Ma et al. 2008; Tuladhar and Mackley 2008; Miller and Cooper-White 2009; Clasen 2010; Arnolds et al. 2010; Vadiillo et al. 2010, 2012; Campo-Deaño and Clasen 2010; Sachsenheimer et al. 2012). Assuming, that the force in the filament is only caused by the surface tension, i.e., no axial normal stresses are considered ( $\sigma_{zz} = 0$ ), the diameter vs. time curve is given by

$$D(t) = D_1 \left( \frac{GD_1}{2\Gamma} \right)^{1/3} \exp\left(-\frac{t}{3\lambda_e}\right) \quad (2)$$

where  $D_1$  is the filament diameter at the time when the exponential filament thinning sets in (this corresponds to time  $t = 0$  in the model equation),  $G$  is the elastic modulus, and  $\lambda_e$  is the so-called elongational relaxation time which depends on polymer concentration. The prefactor in Eq. 2 can differ if the  $\sigma_{zz} = 0$  assumption is not fulfilled (Clasen et al. 2006a). Evaluating the elongational relaxation time  $\lambda_e$  seems to be easy, but technically it is not always unambiguous. Generally, the exponential decay in the diameter vs. time curves occurs at an intermediate stage of filament thinning. Purely viscous stresses dominate initially, while finite extensibility leads to an accelerated filament decay prior the filament breakup (Entov and Hinch 1997). For entangled polymer solutions, the exponential thinning region is barely observable (Clasen 2010) or even completely absent (Arnolds et al. 2010; Sachsenheimer et al. 2012) even if the filament shape still remains cylindrical.

The elongational relaxation time  $\lambda_e$  has been compared to a mean shear relaxation time defined as follows (Liang and Mackley 1994):

$$\bar{\lambda}_s = \frac{\sum 3g_i \lambda_i}{\sum g_i} \quad (3)$$

which is calculated from the relaxation time spectrum which can be obtained from small amplitude oscillatory shear (SAOS) experiments without assuming a specific constitutive equation. However, the comparison with  $\lambda_e$  was not satisfactory: for a series of polyisobutylene (PIB) solutions; they found  $\lambda_e \approx 3\bar{\lambda}_s$  but for the fluid S1,  $\lambda_e \approx 15\bar{\lambda}_s$ .

From a theoretical point of view, Entov and Hinch (1997) analyzed the effect of a relaxation time spectrum on the capillary thinning of viscoelastic filaments using a multimode FENE model. For the so-called middle elastic times resulting in a diameter decay given according to

$$D(t) = D_1 \left[ \frac{D_1}{2\Gamma} \sum_{i=1}^N g_i \exp\left(-\frac{t}{\lambda_i}\right) \right]^{1/3} \quad (4)$$

where  $g_i$  and  $\lambda_i$  are the strength and time parameter of the  $i$ -th component of the relaxation time spectrum and  $N$  is the number of elements. However, it is obvious that a simple exponential filament thinning as observed for, e.g., weakly viscoelastic polymer solutions, can only be observed if all modes  $i > 1$  are relaxed and (4) reduces to Eq. 2 with  $\lambda_e \equiv \lambda_1$  (longest relaxation time of the spectrum). The difference between the diameter calculated from Eqs. 4 and 1 is indeed decreasing with time and less than 5 % for times  $t > 2.5\lambda_1$ . Therefore, the higher modes should only affect the initial nonexponential thinning process. Using polystyrene-based Boger fluids, Anna and McKinley (2001a) also showed the equivalence of the Zimm relaxation time  $\lambda_Z$  as, e.g., defined in Rubinstein and

Colby (2003) and the elongational relaxation time determined from the exponential diameter decay. However, more detailed experimental studies have found relaxation time ratios  $\lambda_e/\lambda_Z = 0.1 \dots 30$  for polyethylenoxied (PEO) and polystyrene (PS) solutions with concentrations  $c \leq c^*$ , where  $c^*$  is the critical overlap concentration (Christanti and Walker 2001; 2002; Tirtaatmadja et al. 2006; Clasen et al. 2006a; Campo-Deano and Clasen 2010; Vaddillo et al. 2012; Haward et al. 2012a). For concentrations  $c \leq c^*$ , relaxation time ratios  $\lambda_e/\lambda_Z = 1 \dots 100$  have been reported (Rodd et al. 2005; Clasen 2010; Haward et al. 2012a) for different polymer solutions.

Finally,  $\lambda_e$  has been related to the terminal shear relaxation time  $\lambda_s$  estimated from SAOS in the terminal flow region ( $\omega \rightarrow 0$ ) according to

$$\lambda_s = \lim_{\omega \rightarrow 0} \frac{G'}{\omega G''} \quad (5)$$

$\lambda_e/\lambda_s \leq 1$  values have been documented for PEO and PS solutions with concentrations  $c^* < c < c_e$  (Oliveira et al. 2006; Arnolds et al. 2010; Clasen 2010) where  $c_e$  is the entanglement concentration. Arnolds et al. (2010) have quantified the effect of nonlinear deformation in CaBER experiments using a single factorizable integral model including a damping function which has been determined from steady shear data. The decrease of the  $\lambda_e/\lambda_s$  ratio with increasing polymer concentration could be predicted quantitatively.

In short, the elongational relaxation time has been compared to different molecular and shear relaxation times, but no simple and universal correlation between these values could be found. However, different shear relaxation times differ from each other. Using the well-known expressions for  $G'$  and  $G''$  of the multimode Maxwell model with discrete relaxation time spectrum ( $g_i, \lambda_i$ ), the terminal shear relaxation time defined by Eq. 5 reads

$$\lambda_{s,Max} = \frac{\sum g_i \lambda_i^2}{\sum g_i \lambda_i} = \frac{\sum g_i \lambda_i^2}{\eta_0}, \quad (6)$$

where  $\eta_0 = \sum g_i \lambda_i$  is the zero shear viscosity. Accordingly,  $\lambda_s$  can be interpreted as the centroid of the relaxation time distribution (Böhme 2000). Obviously,  $\lambda_{s,Max}$  (given by Eq. 6) differs from the mean shear relaxation time  $\bar{\lambda}_s$  suggested by Liang and Mackley (1994) and also from the longest relaxation time  $\lambda_1$  of the spectrum. Using the complex moduli  $G'$  and  $G''$  of the Rouse and Zimm model (Rubinstein and Colby 2003), the characteristic model time constants can be related to the terminal shear relaxation time (5) according to  $\lambda_R = 2\lambda_s$  and  $\lambda_Z = [1 - 1/(3\nu)]^{-1} \lambda_s$ , respectively. Here,  $\nu$  is the scaling exponent associated with solvent quality.

Determination of the elongational viscosity from capillary thinning experiments

The uniaxial elongational viscosity  $\eta_e$  is generally defined as follows (Schuemmer and Tebel 1983):

$$\eta_e = \frac{\sigma_{zz} - \sigma_{rr}}{\dot{\epsilon}}, \quad (7)$$

where  $\sigma_{zz}$  is the axial normal stress in the fluid filament,  $\sigma_{rr}$  is the radial normal stress, and  $\dot{\epsilon}$  is the elongational rate.

Taking into account mass conservation as well as axial and radial force balances on a cylindrical filament undergoing elongation but neglecting gravity and inertia effects, (7) yields (Sachsenheimer et al. 2012)

$$\eta_e = \frac{\Gamma}{dD/dt} - \frac{2F}{\pi D dD/dt}, \quad (8)$$

where  $\Gamma$  is the surface tension, and  $F$  the axial force in the filament with diameter  $D$ . Unfortunately,  $F$  is not measured in standard CaBER experiments. Instead,  $\sigma_{zz} = 0$  is assumed, and the axial force is calculated from the surface tension alone ( $F = \pi D\Gamma$ ). This results in a simplified expression for the elongational viscosity, the so-called apparent elongational viscosity (Anna and McKinley 2001a)

$$\eta_{e,app} = -\frac{\Gamma}{dD/dt} \quad (9)$$

which is widely used in the literature (Rothstein 2003; Yesilata et al. 2006; Oliveira et al. 2006; Bhardwaj et al. 2007a; Sattler et al. 2007; Chellamuthu and Rothstein 2008; Kheirandish et al. 2008; Tuladhar and Mackley 2008; Chen et al. 2008; Yang and Xu 2008; Kheirandish et al. 2009; Arratia et al. 2009; Miller and Cooper-White 2009; David et al. 2009; Regev et al. 2010; Bischoff White et al. 2010; Clasen 2010; Becerra and Carvalho 2011; Erni et al. 2011; Rathfon et al. 2011; Nelson et al. 2011; Haward et al. 2012a; Haward and McKinley 2012b; Gier and Wagner 2012; Tembelya et al. 2012; Vadillo et al. 2012; Sankaran and Rothstein 2012).

Deviations from the  $\sigma_{zz} = 0$  assumption obviously occur for Newtonian liquids (Liang and Mackley 1994; Kolte and Szabo 1999; McKinley and Tripathi 2000; Sachsenheimer et al. 2012) and polymer solutions (Clasen et al. 2006a; Sachsenheimer et al. 2012), and this may be quantified using the dimensionless force ratio (McKinley and Tripathi 2000; Sachsenheimer et al. 2012)

$$X = \frac{F}{\pi D\Gamma}, \quad (10)$$

where  $\pi\Gamma D$  is the force due to the surface tension of the liquid and the  $\sigma_{zz} = 0$  assumption is fulfilled as long as the force ratio is  $X = 1$ . However, the tilted CaBER method can

be used by measuring the true elongational viscosity  $\eta_e$  from CaBER experiments using Eq. 8 without any assumptions.

## Measurement techniques

### Capillary thinning (CaBER) measurements

We have used the commercially available Haake CaBER 1 (Thermo Scientific, Karlsruhe, Germany) for our elongational measurements. The fluid under test is placed between two plates of diameter  $D_0 = 6 \text{ mm}$ . At time  $t = t_0$ , a liquid bridge is created by separating the upper plate from a initial displacement  $h_i$  to a final displacement  $h_f$  within a constant strike time of  $t_s = 40 \text{ ms}$  using a linear stretching profile (constant velocity). Plate separation parameters have been varied between  $0.51 \text{ mm} < h_i < 3 \text{ mm}$  and  $7.4 \text{ mm} < h_f < 12 \text{ mm}$ . At time  $t_1 = t_0 + t_s$ , the liquid thread with an initial diameter of  $D_1 = D(t_1)$  begins to thin due to the acting surface tension until the filament breaks. Filament shapes were captured using an optical setup including a high-speed camera and telecentric illumination (Niedzwiedz et al. 2009; Sachsenheimer et al. 2012). In order to determine the axial force in the filament, the whole CaBER setup has been rotated by  $90^\circ$ . Horizontal filament stretching experiments have always been performed with  $h_i = 0.75 \text{ mm}$  and  $h_f \approx 11.5 \text{ mm}$ . The axial force  $F$  was calculated from the bending line  $w$  of the liquid filament (Sachsenheimer et al. 2012) according to

$$F = \frac{\pi\rho g}{4w} \int_0^x \int_0^{\tilde{x}} D(\hat{x})^2 d\hat{x} d\tilde{x}, \quad (11)$$

where  $\rho$  is the density and  $g$  is the gravitational constant.

For analyzing wormlike micelle solutions, the experimental setup with a resolution of  $16 \mu\text{m}$  has been changed using a mirrorless interchangeable-lens camera (Nikon 1 V2) with a 14-megapixel image sensor yielding a resolution of  $2.5 \mu\text{m}$ . Gentle stretching conditions with  $h_i = 1 \text{ mm}$  and  $h_f = 8 \text{ mm}$  have to be selected in order to create a filament. A higher initial stretching would not yield a homogenous liquid thread.

### Temperature control unit

In order to investigate polymer solutions at different temperatures, a special temperature control unit has been constructed. It consists of a temperature chamber mounted on the CaBER device as shown in Fig. 1 and a temperature sensor installed in the CaBER bottom plate next to the sample. Special glass windows allow for capturing the filament shape using our optical setup as described above and recording the diameter as a function of time using the laser

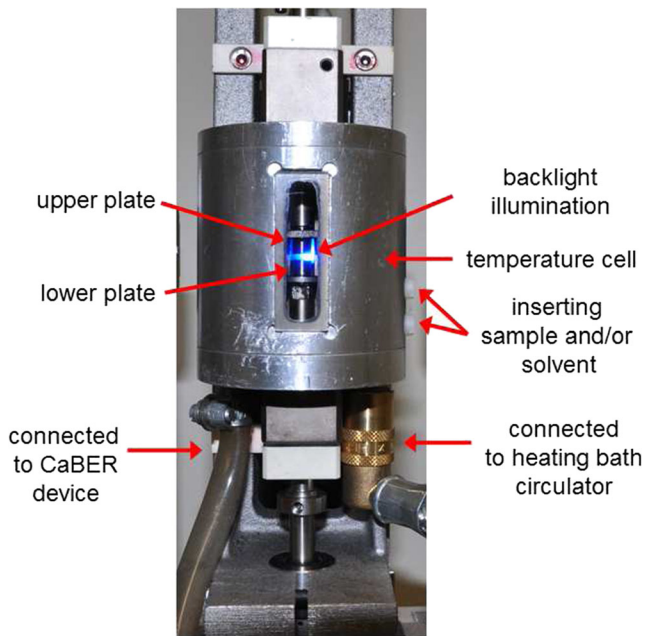


**Fig. 1** Picture of the temperature cell mounted on a CaBER device

micrometer of the device. The cell can also act as a solvent trap. Therefore, solvent is filled into the cell creating a saturated atmosphere to prevent evaporation of solvent from the fluid filament even at elevated temperatures or long filament lifetimes. In contrast to the oven of Bach et al. (2003) where several electric heating elements have been used, our temperature control unit is connected to a water bath thermostat. This allows for a very precise temperature adjustment between 5 and 90°C with an accuracy of 0.2°C.

#### Supplementary measurements

Zero shear viscosity  $\eta_0$  and the longest relaxation time (according to Eq. 5) were determined from SAOS experiments using a Physica MCR501 (Anton Paar, Graz, Austria) equipped with a cone-plate geometry (50 mm diameter and 1° cone angle). Surface tension  $\Gamma$  has been determined at  $T = 20^\circ\text{C}$  using a DCAT1 tensiometer (Data-Physics, Filderstadt, Germany) equipped with a platinum-iridium Wilhelmy plate within an experimental error of  $\Delta\Gamma = \pm 1 \text{ mN/m}$ . Density measurements have been performed using a pycnometer with a total volume of  $V = 10.706 \text{ cm}^3$  at  $T = 20^\circ\text{C}$ .

#### Sample preparation and characterization

PS, PEO, and cetylpyridinium chlorid/sodium salicylate/sodium chloride (CPyCl/NaSal/NaCl) solutions have been used as model systems to study the elongational behavior of viscoelastic, semi-dilute, and concentrated polymer

solutions ( $c > c^*$ ). Polystyrene (Polymer Standards Service, Mainz, Germany) with a weight average molecular weight of  $M_w = 3 \cdot 10^6 \text{ g/mol}$  and a polydispersity index of  $PDI = 1.17$  has been dissolved in diethyl phthalate (Merck, Darmstadt, Germany) with a zero shear viscosity of  $\eta_0 = 12.6 \pm 0.3 \text{ mPas}$ . Polyethylene oxide (Sigma-Aldrich, MO, USA) with weight average molecular weight of  $M_w = 1 \cdot 10^6 \text{ g/mol}$ ,  $M_w = 2 \cdot 10^6 \text{ g/mol}$ , and  $M_w = 4 \cdot 10^6 \text{ g/mol}$  has been dissolved in distilled water. Additionally, aqueous solutions of a low molecular weight PEO ( $M_w = 3.5 \cdot 10^4 \text{ g/mol}$ , in the following labeled as PEG) with concentrations  $c = 8 \%$  ( $\eta_0 = 17.3 \pm 0.1 \text{ mPas}$ ) and  $c = 16.7 \%$  ( $\eta_0 = 97.0 \pm 0.5 \text{ mPas}$ ) have been used as a solvent for the PEO sample with  $M_w = 1 \cdot 10^6 \text{ g/mol}$ . Aqueous PEO solutions are in the  $\theta$ -state at room temperature. Therefore, adding PEG will not change the solvent quality. All polymer solutions were prepared by adding the polymer powder to the solvent. Samples were homogenized by means of shaking at room temperature until the solutions become totally clear. Long shaking times of approximately 1 month were needed for the highly concentrated PS solutions. The surfactant solution CPyCl/NaSal/NaCl is common model systems for linear wormlike micelles (WLM) in the entangled state and corresponding linear viscoelastic data are, e.g., given by Berret et al. (1993). In addition to the reptation time scale  $\lambda_{rep}$  of covalently bounded polymers, WLM break and reform with a characteristic time  $\lambda_{br}$ . For  $\lambda_{br} \ll \lambda_{rep}$ , the rheological behavior is described by a single Maxwell model with relaxation time  $\lambda_s = \sqrt{\lambda_{br}\lambda_{rep}}$  (Rehage and Hoffmann 1988; Cates 1987; 1988). The CPyCl/NaSal/NaCl solutions have been prepared following Berret et al. (1993) at molar surfactant concentrations between 40 and 120 mM and constant salt surfactant ratio of  $R = 0.5$ . A 0.5-M NaCl solution has been used as solvent to ensure a constant electrostatic screening length while varying the CPyCl and NaSal concentrations. NaSal is strongly binding to the surfactant, and both CPyCl and NaSal are responsible for the creation of the wormlike structures. Therefore, we have calculated the living polymer concentration  $c$  as the sum of the mass concentrations of CPyCl and NaSal.

Viscoelastic behavior can be observed in a CaBER experiment if the time scale of the elastically controlled thinning (assumed to be the terminal shear relaxation time  $\lambda_s$ ) exceeds the viscous time scale (assumed to be  $t_v = \eta_0 D / 2\Gamma$ ) quantified using the dimensionless elasto-capillary number (Anna and McKinley 2001a; Clasen 2010):

$$Ec = \frac{2\lambda_s\Gamma}{\eta_0 D}. \quad (12)$$

Since the diameter  $D$  is a function of time, hence the elasto-capillary number is a function of time, too. Figure 2

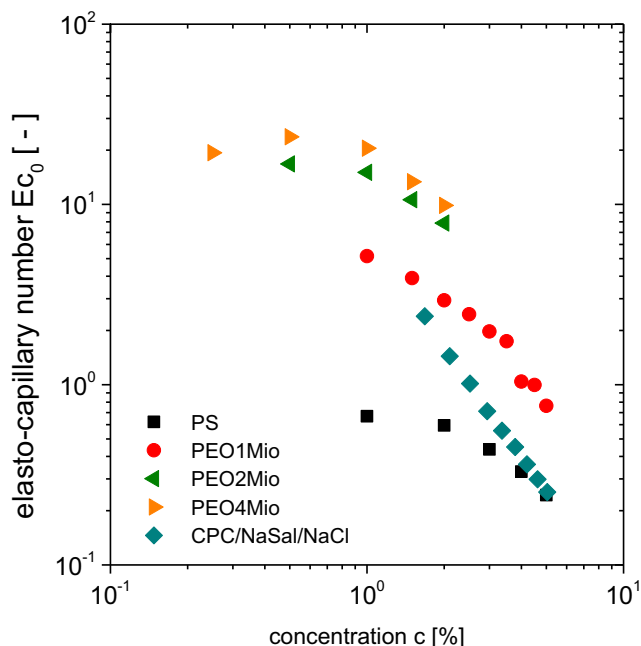


**Fig. 2** Initial elasto-capillary number as a function of polymer concentration for solutions (squares), aqueous PEO solutions with  $M_w = 1 \cdot 10^6$  g/mol (circles), aqueous PEO solutions with  $M_w = 2 \cdot 10^6$  g/mol (diamonds), aqueous PEO solutions with  $M_w = 4 \cdot 10^6$  g/mol (triangles), and CPyCl/NaSal/NaCl (hexagons)

shows the minimum elasto-capillary number  $Ec_0$  calculated using the initial diameter of  $D_0 = 6$  mm for PS, aqueous PEO, and CPyCl/NaSal/NaCl solutions investigated in this study. The elasto-capillary number  $Ec$  decreases with increasing polymer concentration in good agreement with that in the literature (Clasen 2010; Sachsenheimer et al 2012) since the zero shear viscosity varies stronger with polymer concentration than the shear relaxation time. For low polymer concentrations,  $Ec$  is nearly constant. The critical concentration where  $Ec$  begins to decrease is equal to the entanglement concentration  $c_e$  determined from shear viscosity data. These values are summarized in Table 1.

CPyCl/NaSal/NaCl solutions investigated here do not show a constant  $Ec$  value for low concentrations, indicating that all surfactant solutions are in the entangled state.

However,  $Ec_0 < 1$  values may indicate that the beginning of the thinning process is controlled by viscous forces

**Table 1** Entanglement concentrations  $c_e$  and intrinsic viscosities  $[\eta]$

Material	Entanglement concentration $c_e$ /%	Intrinsic viscosity $[\eta]/\text{cm}^3 \text{g}^{-1}$
PS	2.5	295
PEO 1Mio	1.7	598
PEO 2Mio	1.3	1,027
PEO 4Mio	0.66	1,764

instead of viscoelastic as suggested by Clasen (2010) for PS solutions.

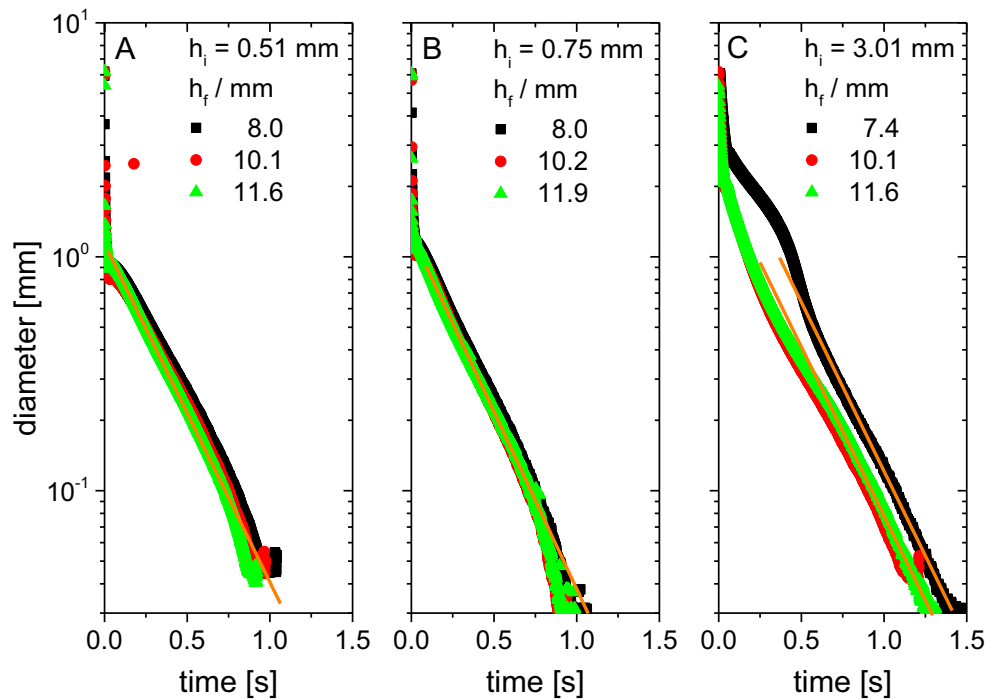
## Results and discussion

### Effect of stretching ratio on the diameter vs. time curve

Low initial heights  $h_i$  and high final heights  $h_f$  are needed for horizontal filament stretching experiments in order to create a measurable deflection of the liquid thread and prevent liquid dropping out of the initial gap of the plates. Dramatically changing of the stretching parameter might influence the thinning behavior of a liquid thread. In addition to Miller et al. (2009) and Kim et al. (2010), we studied these effects using PEG/PEO solutions. Figure 3 shows exemplarily the diameter vs. time curve for 1 % PEO of  $M_w = 1 \cdot 10^6$  g/mol dissolved in a 16.7 % PEG solution using different initial ( $h_i = 0.51$  mm,  $h_i = 0.75$  mm, and  $h_i = 3.01$  mm) and final heights ( $h_f \approx 8$  mm,  $h_f \approx 10$  mm, and  $h_f \approx 12$  mm). Filament lifetime  $t_{fil}$  increases with increasing initial height  $h_i$ ,  $h_i$  but significant differences between  $h_i = 0.51$  mm and  $h_i = 0.75$  mm cannot be observed. The highest filament lifetimes are observed for the lowest stretching ratio ( $h_i = 3.01$  mm and  $h_f = 7.4$  mm). Differences in  $t_{fil}$  might be due to differences in the capillary stress  $\sigma_{rr}(t_1) = -2\Gamma/D_1$  right after the upper plate has reached the end position. Higher filament lifetimes correspond to higher  $D_1$  values (see, for example, Fig. 3c) and therefore to lower initial radial stresses.

An exponential decrease of the filament diameter is clearly and easily visible allowing for a determination of the elongational relaxation time  $\lambda_e$  according to Eq. 2. However, for higher polymer concentrations, the onset of the exponential decay regime is shifted to lower diameters and  $\lambda_e$  can only be determined in the final stage of thinning close to filament breakup. Finally, at concentrations  $c > 4$  % (Arnolds et al. 2010), the exponential diameter decay is no longer observable. In these solutions, a high force ratio  $X > 1$  is present (Sachsenheimer et al. 2012) during the whole thinning process. But for solutions with increased solvent viscosity (added PEG),  $\lambda_e$  can be determined from exponential filament thinning up to 5 % (8 % PEG). Nevertheless, all experiments yield an identical value for the elongational relaxation time independent of  $h_i$  and  $h_f$  in agreement with those in the literature (Kim et al. 2010; Miller et al. 2009). The diameter  $D_{exp,0}$  where the filament begins to thin exponentially decreases with increasing stretching ratio. Therefore, the elasto-capillary number  $Ec$  at which the exponential decrease sets in is not a material parameter as suggested by Clasen (2010) but also depends on the choice of  $h_i$  and  $h_f$ .

**Fig. 3** Filament diameter as a function of time for a 1 % PEO of  $M_w = 1 \cdot 10^6 \text{ g/mol}$  dissolved in a 16.7 % PEG solution with given initial and final heights



Transient force ratio and its relation to the elongational viscosity

Figure 4 shows typical results for a 2 % PEG/PEO and a 4 % PS solution for the force ratio  $X$  as a function of

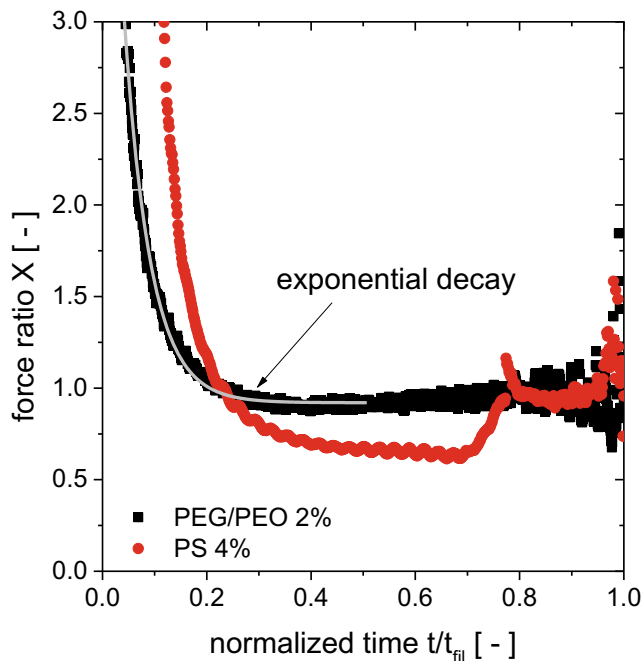


**Fig. 4** Transient force ratio  $X$  as a function of normalized time for a 2 % PEO of  $M_w = 1 \cdot 10^6 \text{ g/mol}$  dissolved in a 16.7 % PEG solution and a 4 % PS solution. The gray line illustrated the exponential decay in the force ratio fitting (15) with  $\tilde{X} = X_\infty$  to the experimental data

the normalized time  $t/t_{fil}$ , where  $t_{fil}$  is the filament lifetime. The force ratio decreases exponentially at the early state of the thinning process, indicating a characteristic initial relaxation process. The sudden separation of the lower and upper plates provokes a huge and rapid deformation of the liquid thread. The diameter of the filament decreases from the initial diameter  $D_0 = 6 \text{ mm}$  to a diameter  $D_1 \approx 1 \text{ mm}$  observed right after the upper plate has reached its final position corresponding to an initial Hencky strain of  $\epsilon_0 \approx 3.6$ . For a typical strike time of  $t_s = 40 \text{ ms}$ , the initial deformation occurs at an average elongation rate  $\langle \dot{\epsilon}_0 \rangle = \epsilon_0/t_s \approx 90 \text{ s}^{-1}$ . This initial step strain results in an (initial) axial normal stress  $\sigma_{zz}$  which relaxes after the step strain. For PEO solutions with low polymer concentrations  $c \leq 2.5 c_e$ , the transient force ratio  $X(t)$  levels off to a final value of  $X_\infty = 1.00 \pm 0.04$  independent of concentration. For higher PEO concentrations, the force ratio  $X_\infty$  increases monotonically with polymer concentration and the exponentially decreasing diameter region is no longer observed (Arnolds et al. 2010; Sachsenheimer et al. 2012). A force ratio  $X = 1$  corresponds to a vanishing axial normal stress  $\sigma_{zz}$  and, therefore, to an axial force  $F$  only given by the surface tension  $\Gamma$  and the diameter  $D$  of the liquid thread.

The PS and CPyCl/NaSal/NaCl solutions show a more complex behavior. After the initial decrease, the transient force ratio levels off to a much lower value of  $X_{min} = 0.75 \pm 0.05$  for PS and CPyCl/NaSal/NaCl independent of the concentration (except of the 1 % PS solution for which the force signal is too low and no  $X_{min}$  could be

detected). These values agree well with the theoretical value of  $X_{New} = 0.713$  for a Newtonian liquid (Papa-georgiou 1995). A force ratio  $X < 1$  corresponds to a compressive axial normal stress  $\sigma_{zz}$  in the fluid filament (Sachsenheimer et al. 2012). After passing the  $X_{min}$  region, the force ratio starts to increase to a final force ratio of  $X_{\infty} = 0.98 \pm 0.08$  for all PS and CPyCl/NaSal/NaCl solutions investigated here. These force measurements confirm the occurrence of an early visco-capillary-controlled regime and a transition to an elasto-capillary-controlled regime for PS and CPyCl/NaSal/NaCl solutions as suggested by Entov and Hinch (1997) as well as by Clasen (2010). The visco-capillary thinning regime occurs due to the low elasto-capillary numbers of these solutions. However, changing the solvent viscosity of PEO solutions by adding PEG does not cause an early Newtonian thinning regime. The viscosity of 16.7 % PEG solution is about seven times higher than the viscosity of diethyl phthalate but elasto-capillary numbers  $Ec_0 > 1$  are found independent of solvent viscosity  $\eta_{sol}$ .

The elongational viscosity  $\eta_e$  is often calculated as apparent value  $\eta_{e,app}$  using the  $\sigma_{zz} = 0$  assumption (corresponding to  $X = 1$ ) according to Eq. 9. Generally, the elongation rate  $\dot{\epsilon}$  changes during capillary thinning in CaBER experiments, but it remains constant for a liquid thread with exponentially decreasing diameter. Then, the elongation rate is related to the elongational relaxation time according to  $\dot{\epsilon} = 2/(3\lambda_e)$ . The normal stresses  $\sigma_{zz}$  and  $\sigma_{rr}$  (if present) also depend on time. In consequence, the elongational viscosity  $\eta_e$  or  $\eta_{e,app}$  are transient values even if the elongation rate  $\dot{\epsilon}$  is constant.

Figure 5 shows exemplarily the true and apparent elongational viscosity as a function of time  $t$  for the 3 % PEG/PEO and the 4 % PS solution. In the first thinning period,  $\eta_e$  decreases with time according to the decrease of the force ratio  $X(t)$ , whereas  $\eta_{e,app}$  increases monotonically. As the capillary thinning proceeds further, the transient elongational viscosity  $\eta_e$  goes through a distinct minimum with  $\eta_{e,min}$  and finally increases exponentially as expected for a Maxwell fluid with a single relaxation time. This strain hardening is a consequence of the well-known entropy elasticity of polymer chains. During this last stage of thinning,  $\eta_{e,app}$  and  $\eta_e$  are equal as expected for  $X = 1$ . Similar results are found for all solutions investigated in this study. For the PS and CPyCl/NaSal/NaCl solutions, the intermediate regime is controlled by visco-capillary thinning ( $X = 0.713$ ) as discussed above yielding an apparent elongational viscosity substantially higher than the true value.

The differences between true and apparent elongational viscosities are caused by the axial normal stress  $\sigma_{zz}$  in the filament which can be expressed in terms of the force ratio

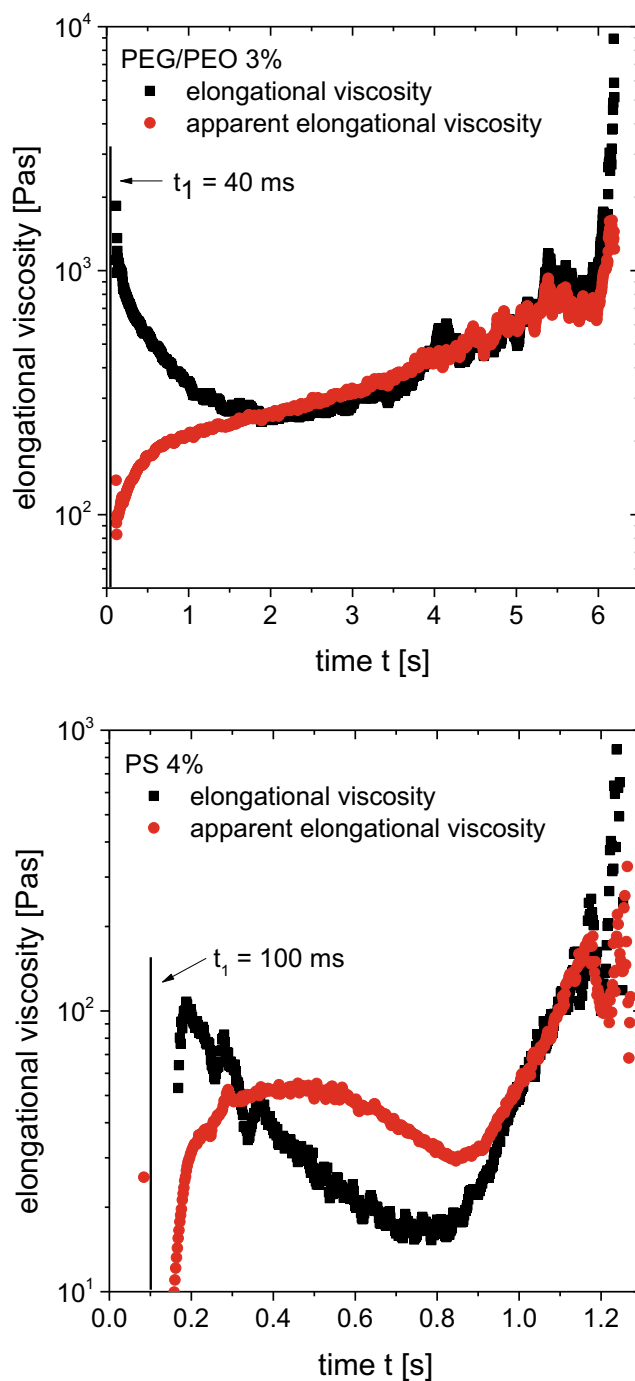


**Fig. 5** Elongational viscosity (squares) and apparent elongational viscosity (circle) as a function of time for a 3 % PEO of  $M_w = 1 \cdot 10^6$  g/mol dissolved in a 16.7 % PEG solution (top) and a 4 % PS (bottom) solution

$X$  and the radial normal stress  $\sigma_{rr}$  according to the following (Sachsenheimer et al. 2012):

$$\sigma_{zz} = 2\sigma_{rr} (1 - X). \quad (13)$$



The ratio of the true elongational viscosity and the apparent elongational viscosity then reads as follows:

$$\frac{\eta_e}{\eta_{e,app}} = \frac{\sigma_{zz} - \sigma_{rr}}{-\sigma_{rr}} = 2X - 1. \tag{14}$$

From Eq. 14, it becomes obvious that a force ratio  $X < 1$ , as observed for a Newtonian controlled thinning, results in an elongational viscosity smaller than the apparent value and  $X > 1$ , as, e.g., observed during the initial period of thinning or for highly concentrated PEO solutions (Sachsenheimer et al. 2012), causes  $\eta_e > \eta_{e,app}$ . Both elongational viscosities (true and apparent) are only equal if the force ratio is  $X = 1$ .

In addition, the uniaxial elongational viscosity of polymer solutions can be obtained from filament stretching extensional rheometer (FiSER) measurements. In such an experiment, the liquid under test is also placed between two parallel plates, but the upper plate is separated continuously until the filament breaks (Tropea et al. 2007). Generally, two types of velocity profiles are possible (Kolte et al. 1997): The upper plate is separated with an exponentially increasing velocity or the plate velocity is controlled, such that the filament diameter decreases exponentially corresponding to a constant elongational rate during the whole experiment (Kolte et al. 1997; Tropea et al. 2007). The transient elongational viscosity is computed from the tensile force exerted by the fluid column on the endplate and the filament diameter at the axial midpoint (McKinley et al. 2001). More details about FiSER are given by Tirtaatmadja and Sridhar (1993); Spiegelberg et al. (1996); Anna et al. (1999, 2001b); Orr and Sridhar (1999); McKinley et al. (2001); McKinley and Sridhar (2002); Rothstein and McKinley (2002a; 2002b); Rothstein (2003), and Tropea et al. (2007).

However, FiSER measurements yield higher values for the maximum elongational viscosity  $\eta_e^{max}$  than CaBER (Bhardwaj et al. 2007a). Similar results are obtained for CPyCl/NaSal/NaCl solutions investigated in this study (data not shown). The observed differences between both techniques may be explained by the simplified CaBER analysis using the  $\sigma_{zz} = 0$  assumption. But as shown above,  $X = 1$  was found the final period of thinning for WLM solutions. Therefore, the  $\sigma_{zz} = 0$  assumption is fulfilled and cannot be the reason for the differences in  $\eta_e^{max}$ . It seems to be more likely that differences in strain history and failure mechanism affect the material behavior in elongational flow. Indeed, FiSER experiments of the 2.94 % CPyCl/NaSal/NaCl solution show a very high maximum force ratio of  $X_\infty^{FiSER} = D_{min}\sigma_{max}/4\Gamma \approx 60$  and a diameter  $D_{min} \approx 1 \text{ mm}$  at filament rupture, clearly indicating the difference in the thinning mechanism.

Figure 6 shows the minimum viscosity ratio  $Tr_{min} = \eta_{e,min}/\eta_0$  for the investigated polymer solutions as a function of polymer concentration  $c$ . The viscosity ratio  $Tr_{min}$

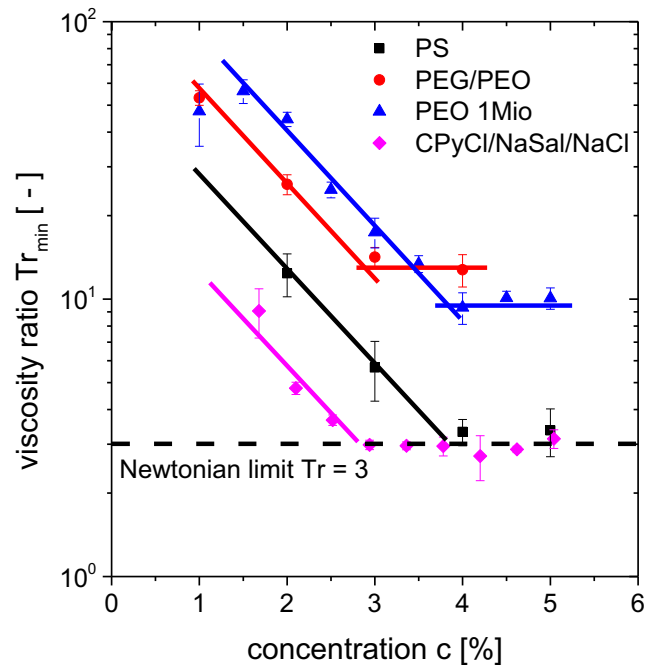


**Fig. 6** Minimum viscosity ratio  $Tr_{min} = \eta_{e,min}/\eta_s$  as a function of concentration for PS (squares), PEO of  $M_w = 1 \cdot 10^6 \text{ g/mol}$  dissolved in a 16.7 % PEG solution (circles), aqueous PEO of  $M_w = 1 \cdot 10^6 \text{ g/mol}$  (triangles), and CPyCl/NaSal/NaCl (diamonds) solutions

decreases exponentially with increasing polymer concentration  $c$  according to  $Tr_{min} \propto \exp(-0.74 \pm 0.02 c/\%)$  and levels off at a constant value for polymer concentrations  $c > c_e$  for all solutions including CPyCl/NaSal/NaCl. For PEO solutions with  $M_w = 1 \cdot 10^6 \text{ g/mol}$ ,  $Tr_{min}$  is between 60 and 70 for low concentrations and levels off to  $Tr_{min} = 9.5 \pm 0.8$ . Obviously, the initial step strain results in a nonlinear change of polymer configuration which does not relax and capillary thinning does not start from the equilibrium where  $Tr = 3$  would be expected. Increasing the solvent viscosity results in a slight increase of  $Tr_{min}$  for high PEO concentrations ( $Tr_{min} = 13.4 \pm 0.8$  for PEO with  $M_w = 1 \cdot 10^6 \text{ g/mol}$  dissolved in an aqueous solution of 16.7 % PEG) and in a similar shift of the concentration at which the limiting value of  $Tr_{min}$  is reached. In contrast, for PS and CPyCl/NaSal/NaCl solutions,  $Tr$  levels off at  $Tr_{min} = 3$ , indicating a relaxation of initial stresses and a pure Newtonian response for high polymer concentrations before the beginning of the elasto-capillary thinning process. Nevertheless, at low concentrations,  $Tr_{min} \gg 3$  is found even though an intermediate Newtonian thinning regime is observed for these solutions.

However, analyzing the minimum Trouton ratio  $Tr_{min}$  seems to be useful due to two reasons. The determination of the minimum elongational viscosity  $\eta_{e,min}$  is very convenient, whereas a determination of the maximum elongational viscosity or maximum Trouton ratio often calculated

for surfactant solutions (Bhardwaj et al. 2007a, b) includes large experimental uncertainties. All solutions (including the CPyCl/NaSal/NaCl surfactant solutions) investigated in this study have thin to very tiny diameters which are hard to be determined accurately. The minimum elongational viscosity also indicates a transition in the thinning behavior. In the initial stage of the experiment, the thinning behavior is controlled by an initial relaxation of the axial normal stress (decrease of  $\eta_e$ ) followed by a pronounced increase of the radial normal stress (increasing of  $\eta_e$ ) at the final stage of thinning.

### Elongational relaxation time

In addition to the determination of elongational viscosities, CaBER experiments also allow for measuring the elongational relaxation time  $\lambda_e$ . Commonly,  $\lambda_e$  is determined from the exponential diameter decay of the liquid filament undergoing capillary thinning according to Eq. 2. Figure 7 shows three independently determined elongational relaxation times for the PEO ( $M_w = 1 \cdot 10^6$  g/mol) and PS solutions investigated in this study: the elongational relaxation time  $\lambda_e$  determined from the diameter vs. time curve of a vertically stretched filament, the elongational relaxation time  $\lambda_e$  determined from the diameter vs. time curve of a horizontally stretched filament, and the force relaxation time  $\lambda_X$  calculated from the initial exponential decay of the transient force ratio in the initial thinning period. Although the filament diameter does not decrease exponentially in this regime, the force ratio follows an exponential decrease in time according to

$$X(t) = C \exp\left(-\frac{t}{\lambda_X}\right) + \tilde{X}, \quad (15)$$

where  $C$  is a constant and  $\tilde{X}$  is the value of the force ratio after the initial decay ( $\tilde{X} \equiv X_\infty \approx 1$  for PEO solutions and  $\tilde{X} \equiv X_{\min} \approx 0.75$  for PS and CPyCl/NaSal/NaCl solutions). A representative result as fit of Eq. 15 to experimental data for 2 % PEO dissolved in the 16.7 % PEG solution is shown as gray line in Fig. 4. We also analyzed the influence of the strike time  $20 \text{ ms} < t_s < 480 \text{ ms}$  on the force relaxation time as shown in the inset of Fig. 7 (top) for the aqueous 4 % PEO ( $M_w = 1 \cdot 10^6$  g/mol) solution. In the investigated parameter range  $\lambda_X$  is found to be independent of the strike time. This indicates that the initial relaxation of the force ratio  $X(t)$  is not influenced by inertia effects as expected since Reynolds numbers defined as  $Re = \rho v D_0 / \eta_0$ , where  $v$  is the velocity of the upper plate during step strain  $v = (h_f - h_i) / t_s$ , are less than one. For the 4 % PEO solution (inset in Fig. 7) with a zero shear viscosity of  $\eta_0 = 8.6 \text{ Pas}$ , the corresponding Reynolds numbers are between 0.016 and 0.38 for strike times varying from 480 and 20 ms. However, considering our standard

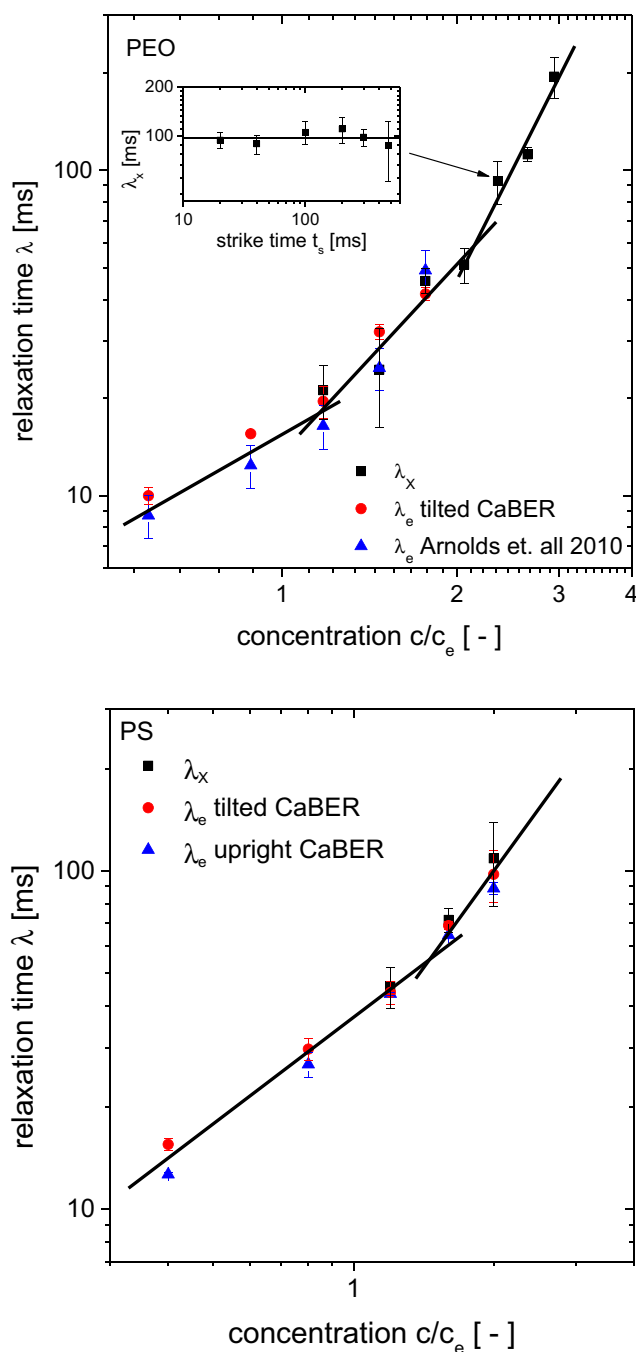


**Fig. 7** Elongational relaxation times from CaBER experiments for aqueous PEO of  $M_w = 1 \cdot 10^6$  g/mol (top) and PS solutions (bottom). Relaxation time values for PEO solutions in the upright CaBER experiment are taken from Arnolds et al. (2010). The inset diagram represents the force ratio relaxation time as a function of the strike time for a 4 % PEO solution. Lines are guide to the eye

setup with  $t_s = 40 \text{ ms}$ , the maximum Reynolds numbers of  $Re = 4$  are found for solutions where a force relaxation time could be determined. But even in these cases, inertia effects may be neglected since the filaments are stabilized elastically (Sachsenheimer et al. 2012).

Nevertheless, too high strike times should not be chosen because a superposition of stretching and capillary thinning has to be avoided. Therefore, we propose an appropriate strike time of  $t_s < 0.1 t_{fil}$ .

All three elongational relaxation times agree well within experimental error irrespective of the polymer concentration as long as  $X_\infty = 1$ . The impressive agreement between  $\lambda_e$  and  $\lambda_X$  suggests that the first stage of capillary thinning, where the diameter does not thin exponentially, is controlled by the same relaxation process as the terminal thinning regime with its exponential filament decay. The excellent agreement between all three relaxation times also shows that gravity has no influence on the elasto-capillary thinning of viscoelastic fluids demonstrating the equivalence of upright and tilted CaBER experiments.

Furthermore, the elongational relaxation times increase monotonically with increasing polymer concentration  $c$ . The force relaxation times  $\lambda$  of PEO solutions with concentrations  $c \geq 4\%$  (corresponding to  $c > 2c_e$ ) show a stronger increase with concentration  $c$  than elongational relaxation times for concentrations  $c < 2c_e$ . However, a determination of  $\lambda$  was not possible for these solutions due to the absence of an exponentially decreasing diameter region (Arnolds et al. 2010). These solutions also exhibit a final force ratio  $X > 1$  (Sachsenheimer et al. 2012).

#### Correlation between shear and elongational relaxation time

In Fig. 8, the relaxation time ratio  $\lambda_e/\lambda_s$  is shown as a function of polymer concentration  $c$ . Data for PEO solutions with different molar masses and solvent viscosities as well as PS solutions at different temperatures are displayed. In all cases, the relaxation time ratio decreases exponentially with increasing polymer concentration  $c$  covering up to 2 orders of magnitude. PEO solutions with higher PEO molar mass show lower  $\lambda_e/\lambda_s$  values (at constant polymer concentration  $c$ ) and a stronger dependence on polymer concentration. Investigations on PEO solutions shows that the solvent viscosity does not affect the relaxation time ratio  $\lambda_e/\lambda_s$ . Varying the temperature of the PS solution between 10 and 40°C corresponds to a viscosity as well as a shear and elongational relaxation time change but does not affect the relaxation time ratio. Slight changes in surface tension or solvent quality upon temperature variation are not considered to be relevant for the  $\lambda_e/\lambda_s$  ratio.

Obviously, changing the solvent viscosity or the temperature affects the relaxation of dissolved polymer molecules in the same way for elongational and shear flows. The elongational relaxation time  $\lambda_e$ , therefore, is a characteristic parameter of the polymer solution but not equal to the terminal shear relaxation time  $\lambda_s$ . Comparing  $\lambda_e$  to a mean shear relaxation time  $\bar{\lambda}_s$  as suggested by Liang and Mackley (1994) according to Eq. 3 requires the knowledge of

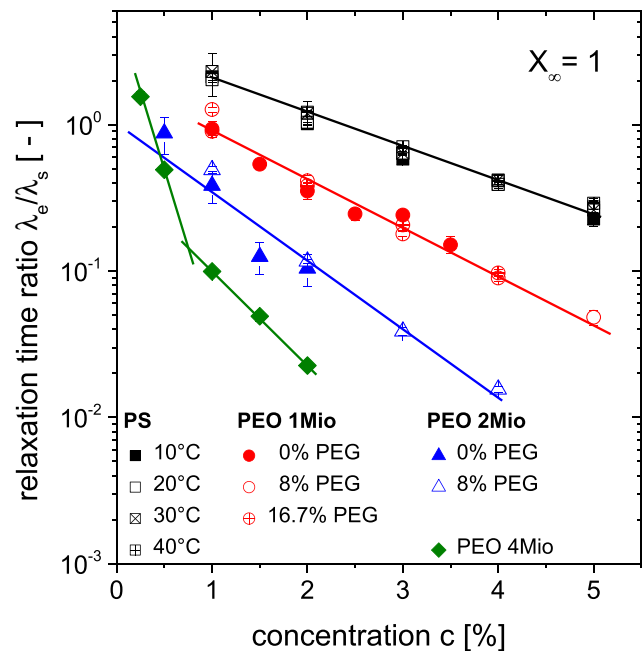


**Fig. 8** Relaxation time ratio as a function of concentration for different polymer solutions with different solvent viscosities and temperatures as shown in the legend of the diagram

the relaxation time spectrum which cannot be determined unambiguously. However, the PS solutions investigated here are thermo-rheologically simple so that the viscosity function  $\eta(\omega)$  of all investigated PS solutions (independent of concentration or temperature) can be plotted as dimensionless master curve by scaling the viscosity with the zero shear viscosity  $\eta_0$  and the angular frequency with the terminal shear relaxation time  $\lambda_s$ . Accordingly, all relaxation times scales with  $\lambda_s$  and any average relaxation time like, e.g.,  $\bar{\lambda}_s$ , exhibit the same dependence on concentration or temperature. As a consequence, the ratio of  $\lambda_e$  and any average relaxation time should be constant independent of concentration or temperature. The strong decrease of  $\lambda_e/\lambda_s$  must therefore be related to a nonlinear material property as already suggested by Arnolds et al. (2010).

Finally, it is interesting to note that the exponential decrease of  $\lambda_e/\lambda_s$  with increasing concentration seems to be a universal feature of entangled polymer solutions. Figure 9 displays the  $\lambda_e/\lambda_s$  values as a function of normalized concentration  $c[\eta]$ , where  $[\eta]$  is the intrinsic viscosity of the polymer solution, for solutions of PEO and PS with different molecular weights, solvent viscosities, and temperatures. Obviously, all data collapse onto a single master curve when plotted as a function of  $c[\eta]$  and follow a unique exponential decay.

For comparison, we have investigated a series of CPyCl/NaSal/NaCl solutions which represent simple Maxwell fluids characterized by one relaxation time (Cates 1996; Berret et al. 1993) as shown in the inset of Fig. 10

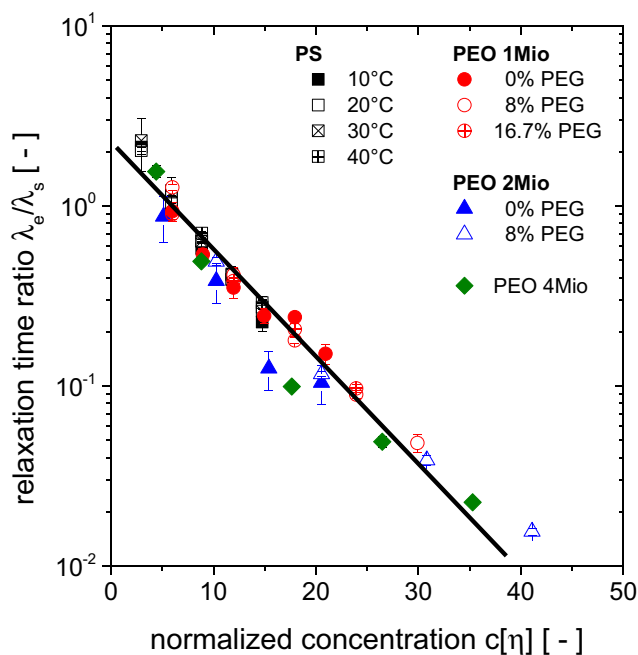


**Fig. 9** Relaxation time ratio as a function of normalized concentration for polymer solutions shown in Fig. 8

where  $G'$  and  $G''$  data for two CPyCl/NaSal/NaCl solutions are shown. Solid lines represent the best fit of the

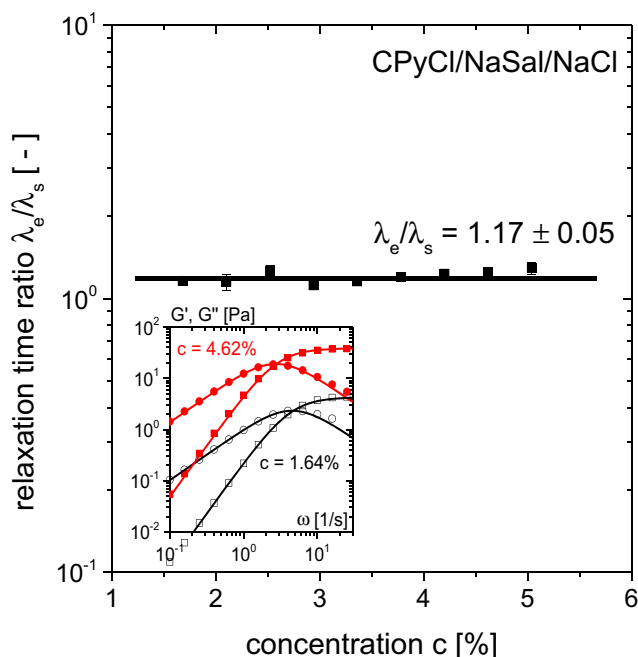


**Fig. 10** Relaxation time ratio as a function of concentration for different CPyCl/NaSal/NaCl solutions. The line represents the relaxation time ratio mean value of  $\lambda_e/\lambda_s = 1.17 \pm 0.05$ . The inset shows the storage (*squares*) and loss modulus (*circles*) as a function of angular frequency for the 4.42 % (*filled symbols*) and the 1.64 % CPyCl/NaSal/NaCl solution (*open symbols*). Best fits of experimental data, using a single Maxwell model, are represented in the inset as *solid lines*

Maxwell model to the experimental data. The relaxation time ratio for these simple Maxwell fluids is shown in Fig. 10. Surprisingly, all solutions show a constant value of  $\lambda_e/\lambda_s = 1.17 \pm 0.05$  independent of concentration, indicating that the elongational behavior of WLM solutions is only given by linear fluid properties determined in small amplitude oscillatory shear. This result is remarkable because the relaxation time of a wormlike structure strongly depends on the mean length of the micelles. Finding  $\lambda_e \approx \lambda_s$  suggests that the mean length does not change during the elongational deformation as discussed theoretically (Vasquez et al. 2007; Cromer et al. 2009; Germann et al. 2013). A change in micellar length due to a deformation-induced increase of the breakage rate would dramatically shorten the relaxation time and  $\lambda_e/\lambda_s \ll 1$  would be expected.

On the other hand,  $\lambda_e \approx \lambda_s$  implies that nonlinear effects are not relevant in CaBER experiments of these surfactant solutions. Identifying the shear relaxation time  $\lambda_s$  as characteristic relaxation time of the material and considering  $\dot{\epsilon} = 2/(3\lambda_e)$ , the relaxation time ratio  $\lambda_e/\lambda_s$  might be interpreted as an inverse Weissenberg number  $Wi^{-1} = (\dot{\epsilon}\lambda_s)^{-1} = 3\lambda_e/(2\lambda_s)$ . For CPyCl/NaSal/NaCl solutions,  $Wi = 0.6$  is independent of surfactant concentration indicating a linear viscoelastic response. Unfortunately, the model of Arnolds et al. (2010) taking into account the strong deformation during capillary thinning cannot be applied here. The damping function cannot be determined from independent steady shear experiments since shear banding is prominent in these flows (Bhardwaj et al. 2007a, b).

## Conclusion

We have investigated capillary thinning of entangled polymer solutions focusing on weakly elastic systems showing exponential diameter decay.

The tilted CaBER method has been used to determine the force ratio  $X$  and the true elongational viscosity  $\eta_e$ . The force ratio decays exponentially and levels off at  $X_\infty = 1$  for the PEO solutions with high elasto-capillary numbers  $Ec_0$ . However, for the PS and CPyCl/NaSal/NaCl solutions with  $Ec_0 \leq 1$ , an intermediate Newtonian thinning regime was confirmed based on the measured force ratio  $X = 0.713$  as already suggested by Clasen (2010). The initial stress decay after step strain filament formation is characterized by a relaxation time  $\lambda_X$  equal to the relaxation time  $\lambda_e$  determined from the terminal exponential thinning region. Obviously, the corresponding initial decrease of the elongational viscosity  $\eta_e$  is controlled by the same molecular processes like the increase of  $\eta_e$  (strain hardening) in the final regime of thinning. Since  $\eta_e$  goes through a distinct minimum during filament thinning, a characteristic minimum Trouton ratio  $Tr_{\min}$  can be determined accurately.

This Trouton ratio decreases exponentially with increasing polymer concentration for all investigated solutions and levels off at  $Tr_{\min} = 10$  for all PEO solutions irrespective of solvent viscosity. For the PS and CPyCl/NaSal/NaCl solutions characterized by low elasto-capillary numbers,  $Tr_{\min} = 3$  is found.

The relaxation time ratios  $\lambda_e/\lambda_s$  decreases exponentially with increasing polymer concentration and the data for all investigates PEO and PS solutions collapse onto a single master curve irrespective of polymer molecular weight, solvent viscosity, or temperature when plotted versus reduced concentration  $c[\eta]$ . This decrease is due to the strong non-linear deformation in CaBER experiments as suggested earlier (Arnolds et al. 2010) but not due to a different weighting of relaxation times in the different flow kinematics.

On the other hand,  $\lambda_e \approx \lambda_s$  is found for all investigated CPyCl/NaSal/NaCl solutions, clearly indicating that nonlinear effects are not relevant in capillary thinning of these “living” polymer systems.

**Acknowledgments** The authors would like to thank Sonja Müller, Sebastian Bindgen, and Frank Bossler for their help in sample preparation and performing the experiments. We would like to thank Jonathan Rothstein and Sunil Khandavalli (University of Massachusetts) for the possibility to use the FiSER setup and for all help given. Financial support by German Research Foundation DFG grant WI 3138/13-1 is gratefully acknowledged.

## References

- Ameri David RL, Wei MH, Kornfield JA (2009) Effects of pairwise, donor–acceptor functional groups on polymer solubility, solution viscosity and mist control. *Polymer* 50(26):6323–6330
- Anna SL, McKinley GH (2001a) Elasto-capillary thinning and breakup of model elastic liquids. *J Rheol* 45:115–138
- Anna SL, McKinley GH, Nguyen DA, Sridhar T, Muller SJ, Huang J, James DF (2001b) An inter-laboratory comparison of measurements from filament stretching rheometers using common test fluids. *J Rheol* 45:83–114
- Anna SL, Rogers C, McKinley GH (1999) On controlling the kinematics of a filament stretching rheometer using a real-time active control mechanism. *J Non-Newton Fluid Mech* 87:307–335
- Arnolds O, Buggisch H, Sachsenheimer D, Willenbacher N (2010) Capillary breakup extensional rheometry (CaBER) on semi-dilute and concentrated polyethylene oxide (PEO) solutions. *Rheol Acta* 49:1207–1217
- Arratia PE, Cramer LA, Gollub JP, Durian DJ (2009) The effects of polymer molecular weight on filament thinning and drop breakup in microchannels. *New Jour of Phys* 11:115–006
- Bach A, Rasmussen HK, Hassager O (2003) Extensional viscosity for polymer melts measured in the filament stretching rheometer. *J Rheol* 47(2):429–441
- Bazilevskii AV, Entov VM et al (1997) Failure of polymer solution filaments. *Polym Sci A* 39:316–324
- Bazilevsky AV, Entov VM, Rozhkov AN (1990) Liquid filament microrheometer and some of its applications. In: Oliver DR (ed) conference, Third European rheology. Elsevier, San Diego, pp 41–43
- Bazilevsky AV, Entov VM, Rozhkov AN (2001) Breakup of an Oldroyd liquid bridge as a method for testing the rheological properties of polymer solutions. *Polym Sci Ser A* 43:716–726
- Becerra M, Carvalho MS (2011) Stability of viscoelastic liquid curtain. *Eng and Proc* 50:445–449
- Berret JF, Appell J, Porte G (1993) Linear rheology of entangled wormlike micelles. *Langmuir* 9:2851–2854
- Bhardwaj A, Miller E, Rothstein JP (2007a) Filament stretching and capillary breakup extensional rheometry measurements of viscoelastic wormlike micelle solutions. *J Rheol* 51:693–719
- Bhardwaj A, Richter D, Chellamuthu M, Rothstein JP (2007b) The effect of preshear on the extensional rheology of wormlike micelle solutions. *Rheol Acta* 46:861–875
- Bischoff White EE, Chellamuthu M, Rothstein JP (2010) Extensional rheology of a shear-thickening cornstarch and water suspension. *Rheol Acta* 49:119–129
- Böhme G (2000) *Strömungsmechanik nichtnewtonischer Fluide*. Teuber, Stuttgart
- Brenner M, Lister J, Stone H (1996) Pinching threads, singularities and the number 0.0304. *Phys Fluids* 8:2827–2836
- Campo-Deaño L, Clasen C (2010) The slow retraction method (SRM) for the determination of ultra-sort relaxation times in capillary breakup extensional rheometry experiments. *J Non-Newton Fluid Mech* 165:1688–1699
- Cates ME (1987) Reptation of living polymers: dynamics of entangled polymers in the presence of reversible chain-scission reactions. *Macromolecules* 20:2289–2296
- Cates ME (1988) Dynamics of living polymers and flexible surfactant micelles: scaling laws for dilution. *J Phys France* 49(9):1593–1600
- Cates ME (1996) Flow behaviour of entangled surfactant micelles. *J Phy: Condensed Matter* 8:9167–9176
- Chellamuthu M, Rothstein JP (2008) Distinguishing between linear and branched wormlike micelle solutions using extensional rheology measurements. *J Rheol* 52:865–884
- Chen L, Bromberg L, Hatton TA, Rutledge GC (2008) Electrospun cellulose acetate fibers containing chlorhexidine as a bactericide 49(5):1266–1275
- Christanti Y, Walker LM (2001) Surface tension driven jet break up of strain-hardening polymer solutions. *J Non-Newtonian Fluid Mech* 100:9–26
- Christanti Y, Walker LM (2002) Effect of fluid relaxation time of dilute polymer solutions on jet breakup due to a forced disturbance. *J Rheol* 46:733–748
- Clasen C, Eggers J, Fontelos MA, Li J, McKinley GH (2006a) The beads on-string structure of viscoelastic threads. *J Fluid Mech* 556:283–308
- Clasen C, Plog JP et al. (2006b) How dilute are dilute solutions in extensional flows *J Rheol* 50:849–881
- Clasen C (2010) Capillary breakup extensional rheometry of semi-dilute polymer solutions. *K-A Rheol J* 22:331–338
- Cromer M, Cook PL, McKinley GH (2009) Extensional flow of wormlike micellar solutions. *Chem Eng Science* 64:4588–4596
- Eggers J (1993) Universal pinching of 3D axisymmetric free-surface flows. *Phys Rev Lett* 71:3458–3490
- Eggers J (1997) Nonlinear dynamics and breakup of free-surface flows. *Rev Mod Phys* 69:865–930
- Entov VM, Hinch EJ (1997) Effect of a spectrum of relaxation times on the capillary thinning of a filament of elastic liquid. *J Non-Newton Fluid Mech* 72:31–53
- Erni P, Varagnat M, Clasen C, Crest J, McKinley GH (2011) Microrheometry of sub-nanolitre biopolymer samples: non-Newtonian flow phenomena of carnivorous plant mucilage. *Soft Matter* 7:10889–10898
- Germann N, Cook LP, Beris AN (2013) Nonequilibrium thermodynamic modeling of the structure and rheology of concentrated

- wormlike micellar solutions. *J Non-Newton Fluid Mech* 196:51–57
- Gier S, Wagner C (2012) Visualization of the flow profile inside a thinning filament during capillary breakup of a polymer solution via particle image velocimetry and particle tracking velocimetry. *Phys Fluids* 24:053–102
- Haward SJ, McKinley GH (2012b) Stagnation point flow of wormlike micellar solutions in a microfluidic cross-slot device: Effects of surfactant concentration and ionic environment. *Phys Rev E* 85:031–502
- Haward SJ, Sharma V, Butts CP, McKinley GH, Rahatekar SS (2012) Shear and extensional rheology of cellulose/ionic liquid solutions. *Biomacromolecules* 13(5):1688–1699
- Kheirandish S, Gubaydullin I, Willenbacher N (2008) Shear and elongational flow behaviour of acrylic thickener solutions. Part I: effect of intermolecular aggregation. *Rheol Acta* 49:397–407
- Kheirandish S, Gubaydullin I et al (2009) Shear and elongational flow behavior of acrylic thickener solutions, Part II: effect of gel content. *Rheol Acta* 48:397–407
- Kim NJ, Pipe CJ, Ahn KH, Lee SJ, McKinley GH (2010) Capillary breakup extensional rheometry of a wormlike micellar solution. *Korea-Aust Rheol J* 22:31–41
- Klein CO, Naue IF et al (2009) Addition of the force measurement capability to a commercially available extensional rheometer (CaBER). *Soft Mater* 7:242–257
- Kolte MI, Rasmussen HK, Hassager O (1997) Transient filament stretching rheometer II: numerical simulation. *Rheol Acta* 36:285–302
- Kolte MI, Szabo P (1999) Capillary thinning of polymeric filaments. *J Rheol* 43:609–626
- Liang RF, Mackley MR (1994) Rheological characterization of the time and strain dependence for polyisobutylene solutions. *J Non-Newton Fluid Mech* 52:387–405
- Ma WKA, Chinesta F, Tuladhar T, Mackley MR (2008) Filament stretching of carbon nano tube suspension. *Rheol Acta* 47:447–457
- Martinie L, Buggisch H, Willenbacher N (2013) Apparent elongational yield stress of soft matter. *J Rheol* 57:627–646
- McKinley GH (2005) Visco-elasto-capillary thinning and breakup of complex fluid. *Rheology Reviews 2005. The British Soc Rheol*:1–49
- McKinley GH, Brauner O, Yao M (2001) Kinematics of filament stretching in dilute and concentrated polymer solutions. *Korea-Australia Rheol J* 13(1):29–35
- McKinley GH, Sridhar T (2002) Filament stretching rheometry. *Annu Rev Fluid Mech* 34:375–415
- McKinley GH, Tripathi A (2000) How to extract the Newtonian viscosity from capillary breakup measurements in a filament rheometer. *J Rheol* 44(3):653–670
- Miller E, Cooper-White J (2009) The effects of chain conformation in the microfluidic entry flow of polymer-surfactant systems. *Non-Newtonian Fluid Mech* 160:22–30
- Münstedt H (1975) Viscoelasticity of polystyrene melts in tensile creep experiments. *Rheol Acta* 14:1077–1088
- Münstedt H (1979) New universal extensional rheometer for polymer melts. *J Rheol* 23:421–436
- Münstedt H, Kurzbeck S, Egersdörfer L (1998) Influence of molecular structure on rheological properties of polyethylenes Part II. Elongational behavior. *Rheol Acta* 37:21–29
- Nelson WC, Kavehpour HP, Kim CJ (2011) A miniature capillary breakup extensional rheometer by electrostatically assisted generation of liquid filaments. *Lab Chip* 11:2424–2431
- Niedzwiedz K, Arnolds O, Willenbacher N, Brummer R (2009) How to characterize yield stress fluids with capillary breakup extensional rheometry (CaBER). *Appl Rheol* 19:41969–1–41969–10
- Niedzwiedz K, Buggisch H, Willenbacher N (2010) Extensional rheology of concentrated emulsions as probed by capillary breakup elongational rheometry (CaBER). *Rheol Acta* 49:1103–1116
- Oliveira MSN, Yeh R, McKinley GH (2006) Iterated stretching, extensional rheology and formation of beads-on-string structures in polymer solutions. *J Non-Newton Fluid Mech* 137:137–148
- Orr NV, Sridhar T (1999) Probing the dynamics of polymer solutions in extensional flow using step strain rate experiments. *J Non-Newton Fluid Mech* 82:203–232
- Papageorgiou DT (1995) On the breakup of viscous liquids threads. *Phys Fluids* 7:1529–1544
- Rathfon JM, Cohn RW, Crosby AJ, Rothstein JP, Tew GN (2011) Confinement effects on chain entanglement in free-standing polystyrene ultrathin films. *Macromolecules* 44(13):5436–5442
- Regeva O, Vandebriel S, Zussmana E, Clasen C (2010) The role of interfacial viscoelasticity in the stabilization of an electrospun jet. *Polymer* 50(12):2611–2620
- Rehage H, Hoffmann H (1988) Rheological Properties of Viscoelastic Surfactant Systems. *J Physl Chem* 92(16):4712–4719
- Renardy M (1994) Some comments on the surface tension driven breakup (or the lack of it) of the viscoelastic jets. *J Non-Newton Fluid Mech* 51:97–107
- Renardy M (1995) A numerical study of the asymptotic evolution and breakup of Newtonian and viscoelastic jets. *J Non-Newton Fluid Mech* 59:267–282
- Rodd LE, Scott TP, Cooper-White JJ, McKinley GH (2005) Capillary breakup rheometry of low-viscosity elastic fluids. *Appl Rheol* 15(1):12–27
- Rothstein JP (2003) Transient extensional rheology of wormlike micelle solutions. *J Rheol* 47:1227–1247
- Rothstein JP, McKinley GH (2002a) A comparison of the stress and birefringence growth of dilute, semi-dilute and concentrated polymer solutions in uniaxial extensional flows. *J Non-Newton Fluid Mech* 108:275–290
- Rothstein JP, McKinley GH (2002b) Inhomogeneous transient uniaxial extensional rheometry. *J Rheol* 46:1419–1443
- Rubinstein M, Colby RH (2003) *Polymer physics*. Oxford University Press, Oxford
- Sachsenheimer D, Hochstein B, Buggisch H, Willenbacher N (2012) Determination of axial forces during the capillary breakup of liquid filaments - the tilted CaBER method. *Rheol Acta* 51:909–923
- Sankaran AK, Rothstein JP (2012) Effect of viscoelasticity on liquid transfer during gravure printing. *J Non-Newtonian Fluid Mech* 175–176:64–75
- Sattler R, Gier S, Eggers J, Wagner C (2012) The final stages of capillary break-up of polymer solutions. *Phys Fluids* 24:023–101
- Sattler R, Kityk A, Wagner C (2007) Molecular configurations in the droplet detachment process of a complex liquid. *Phys Rev E* 75:051805-1-051805-6
- Schümmer P, Tebel KH (1983) A new elongational rheometer for polymer solutions. *J Non-Newtonian Fluid Mech* 12(3):331–347
- Spiegelberg S, Ables D, McKinley GH (1996) Role of end-effects on measurements of extensional viscosity in viscoelastic polymer solutions with a filament stretching rheometer. *J Non-Newton Fluid Mech* 64(2–3):229–267
- Tan L, Pan J, Wan A (2012) Shear and extensional rheology of polyacrylonitrile solution: effect of ultrahigh molecular weight polyacrylonitrile. *Colloid Polym Sci* 290:289–295
- Tembelya M, Vadillo D, Mackley MR, Soucemarianadin A (2012) The matching of a one-dimensional numerical simulation and experiment results for low viscosity Newtonian and non-Newtonian fluids during fast filament stretching and subsequent break-up. *J Rheol* 56:159–183

- Tirtaatmadja V, McKinley GH, Cooper-White JJ (2006) Drop formation and breakup of low viscosity elastic fluids: effects of molecular weight and concentration. *Phys Fluids* 18:043–101
- Tirtaatmadja V, Sridhar T (1993) Filament stretching device for measurement of extensional viscosity. *J Rheol* 36(3):277–284
- Tropea C, Yarin AL, Foss JF (2007) *Springer handbook of experimental fluid mechanics*. Springer, Heidelberg
- Tuladhar TR, Mackley MR (2008) Filament stretching rheometry and break-up behaviour of low viscosity polymer solutions and ink jets fluids. *J Non-Newton Fluid Mech* 148:97–108
- Vadillo D, Mathues W, Clasen C (2012) Microsecond relaxation processes in shear and extensional flows of weakly elastic polymer solutions. *Rheol Acta* 51:755–769
- Vadillo DC, Tuladhar TR, Mulji AC et al (2010) Evaluation of ink jet fluid's performance using the Cambridge TriMASTER filament stretch and breakup-device. *J Rheol* 54(2):261–282
- Vasquez PA, McKinley GH, Cooka LP (2007) A network scission model for wormlike micellar solutions I. Model formulation and viscometric flow predictions. *J Non-Newtonian Fluid Mech* 144:122–139
- Yang J, Xu Y (2008) Coalescence of two viscoelastic droplets connected by a string. *Phys Fluids* 20:043101-1-043101-9
- Yesilata B, Clasen C, McKinley GH (2006) Nonlinear shear and extensional flow dynamics of wormlike surfactant solutions. *J Non-Newton Fluid Mech* 133:73–90